



## The impact of initial conditions on convection-permitting simulations of flood events

Lu Li<sup>1</sup>, Marie Pontoppidan<sup>1</sup>, Stefan Sobolowski<sup>1</sup>, Alfonso Senatore<sup>2</sup>

<sup>1</sup>NORCE Norwegian Research Centre, Bjerknes Centre for Climate Research, Jahnebakken 5, 5008 Bergen, Norway

5 <sup>2</sup>Department of Environmental and Chemical Engineering, University of Calabria, Italy

*Correspondence to:* Lu Li (luli@norceresearch.no)

**Abstract.** Western Norway suffered major flooding after 4 days of intense rainfall during the last week of October 2014, resulting in damages totalling hundreds of millions Norwegian kroner. These types of events are expected to become more frequent and severe as Norwegian (and the earth's) climate continues to warm. However, due to the strong effects that local features and conditions can have on these kinds of events, coarse-grained global or regional models are unable to capture their characteristics. Very high resolution models run at so-called convection-permitting scales have shown some promise for reliably capturing such events. Doing so in a robust manner is, as a matter of course, of high interest to both scientists and stakeholders in both climate prediction and projection contexts. Despite this promise, the impacts of initial conditions on convection-permitting simulations, i.e., precipitation pattern and discharge, are uncertain, especially over complex, mountainous terrain. Complicating matters, these areas also usually lack dense measurement networks. In this paper, we apply a distributed dynamic regional atmosphere-hydrological modelling system (WRF-Hydro) at convection-permitting scale and assess its performance over four catchments in western Norway for the aforementioned flood event. The model is calibrated and then evaluated using observations and benchmarks obtained from the HBV light model. Interestingly, the calibrated WRF-Hydro model with NSE value of 0.86 exceeds the upper benchmark obtained from the conceptual HBV model with NSE value of 0.80 suggesting that the former performs as well or better than the simpler conceptual model, especially in areas with complex terrain and poor observational coverage. Confident in the capabilities of the modelling system we then examined the sensitivity of precipitation pattern and discharge, especially peak flow, to poorly constrained elements such as spinup time and snow conditions. The results show that: (1) overall the convection-permitting WRF-Hydro simulation captures the precipitation pattern/amount, the peak flow volume and the timing of the flood event; (2) precipitation is not overly sensitive to spinup time, while discharge is slightly more sensitive due to the influence of soil moisture, especially during the pre-peak phase; (3) the idealized snow depth experiments show that a maximum of 0.5 m of snow is converted to runoff irrespective of the initial snow depth and that this snowmelt contributes to discharge mostly during the rainy and the peak flow periods. This suggests that snow-cover, in these experiment at least, intensifies the extreme discharge instead of acting as sponge, which further implies that future rain-on-snow events may contribute to



30 higher flood risk. While targeted experiments on the changing characteristics of projected future rain-on-snow events are  
needed to confirm this study suggests that WRF-Hydro is an ideally formulated tool to investigate these questions.

## 1 Introduction

Heavy rainfall, with local amounts exceeding 350 mm, fell over the coastal and mountainous areas of western Norway  
between 26 - 29 October 2014. The event caused widespread flooding, with 16 stations registering discharge above the 50-  
35 year flood threshold (Langsholt et al., 2015). The severe flooding of many regional river systems destroyed infrastructure,  
houses and isolated towns. Overall the damage exceeded 131.6 million Norwegian kroner (Dannevig et al., 2016). A list of  
reports (in Norwegian), e.g. “October flood in western Norway 2014” (Dannevig et al., 2016) and “The flood in western  
Norway October 2014” (Lansholt et al., 2015) from Norwegian Water Resources and Energy Directorate (NVE) were  
produced, which documented the rainfall and discharge records and societal impacts. For flood hazards such as this, it is a  
40 challenge to forecast/hindcast the hydrological response due to the complex terrain and the events’ complex spatial and  
temporal characteristics. However, with extreme precipitation over this region projected to increase significantly over the  
coming decades (e.g. Hanssen-Bauer et al., 2017) the need to reliably reproduce such events is high for both climate  
researchers and operational professionals.

### 1.1 Norwegian flood types, changes & rain-on-snow

45 The complex and varying terrain of Norway divides the country into different climatic zones and flood-generating processes  
vary by regions. For example, northern and eastern Norway are mainly prone to spring snowmelt floods while southern and  
western Norway are dominated by rain induced floods (Vormoor et al., 2015). According to recent studies, snowmelt  
generated floods have decreased and shifted earlier in the spring in recent decades (Vormoor et al., 2016; Pall et al. 2018). At  
the same time, rain dominated floods are increasing in frequency (Vormoor et al., 2016). This is consistent with observed  
50 increases in precipitation (Dyrrdal et al., 2012) and streamflow (Stahl et al., 2010; Wilson et al., 2010), and the trends are  
projected to continue into the future (Hanssen-Bauer et al., 2017; Sorteberg et al., 2018). Though temperatures are  
increasing, much of the winter precipitation in inland catchments will continue to fall as snow until at least the mid-century  
(Hanssen-Bauer et al., 2017). However, as temperature rises many of these catchments may experience more rain-on-snow  
events. Warm, and often windy conditions during such events can cause substantial additional snowmelt, which can  
55 exacerbate an already dangerous flooding event (Marks et al., 1998, 2001). In fact, for many catchments in the world, such  
as the western US, rain-on-snow events are important for prediction of flood responses and risk (Berghuijs et al., 2016;  
Musselman et al., 2018). While earlier snowmelt is decreasing the frequency of such events in the late spring and at low  
altitudes, both the magnitude and frequency of rain-on-snow events are increasing during winter in central Europe (Freudiger



et al., 2014), and likely also in Norway. Pall et al. (2018) used a high-resolution (1 km) seNorge data set to construct  
60 climatology of rain-on-snow occurrence in the mainland Norway for recent decades. They found an increase in rain-on-snow  
events in high-elevation areas across the mainland in winter-spring. Given the dependence of floods in Norway on a complex  
interplay between variations in elevation, temperature gradients (e.g. between land and ocean), orographic interactions,  
existing snow and soil moisture distributions, etc. it is critical to run models (either dynamical or statistical) at resolutions  
that can capture this complexity. But this requirement presents challenges of its own. In addition, few studies have assessed  
65 the causality of flood occurrence (extreme streamflow) resulting from rain-on-snow signals at the local hydrological scale  
(e.g. Surfleet and Tullos, 2013; Corripio and López-Moreno 2017). Despite this, the rain versus snowmelt contribution to the  
flow can be important in determining the flood generation processes for Norway and can be particularly sensitive to the  
vertical temperature gradient.

### 1.2 Forcing data and convection-permitting modelling

70 In order to improve our scientific understanding as well as predictions and projections of flooding, high quality  
meteorological forcing data is crucial. A lack of detailed precipitation records that accurately represent spatial and temporal  
variability at both the basin and regional scales presents well-known challenges to hydrological modelling. In mountainous  
areas, like western Norway, where precipitation is strongly influenced by the terrain, spatial patterns of precipitation are not  
well captured by either sparse gauge data or gridded precipitation datasets (e.g. satellite-based products or high-resolution  
75 interpolation-based datasets). High-resolution, convection-permitting modelling has exhibited great promise in addressing  
these issues and has potential as a powerful tool for hydrological prediction (Prein et al., 2015, 2016, 2017; Smiatek et al.,  
2016; Kendon et al., 2017; El-Samra et al., 2018; Poschlod et al., 2018; Avolio et al., 2019). Pontoppidan et al. (2017)  
investigated the atmospheric conditions leading to the aforementioned flooding event in October 2014 over Western Norway  
and found that convection permitting simulations (~3km grid spacing) from the Weather Research and Forecasting (WRF)  
80 model substantially improved the representation of precipitation compared to a coarser resolution reanalysis. This  
improvement was seen both in terms of absolute values and spatial-temporal distribution. The largest improvement was  
found with the resolution jump from parameterized to explicitly resolved convection (e.g., 9km to 3km over western  
Norway). Several previous studies over other regions also demonstrate the added-value of convection permitting modelling  
for extreme weather impact studies in regions with complex terrain. For example, Maussion et al. (2011) showed improved  
85 representation of precipitation in a convection-permitting (2km) simulation when compared to satellite products over the  
Himalayan region. El-Samra et al. (2018) suggest that downscaling over complex terrain requires a horizontal grid resolution  
of 3km or higher in to improve the forecasting of mean and extreme temperatures and capture the orographic precipitation  
climatology. Conversely, coarse resolution (~ 9km) simulations miss the impact of orography on temperature and  
precipitation. Additionally, the studies of Rasmussen et al. (2011, 2014) found that a spatial and temporal depiction of



90 snowfall that is adequate for water resource management over the Colorado Headwaters regions can only be achieved with the appropriate choice of model grid spacing and parameterizations. The modeling systems that are capable of accurately depicting the atmosphere at these scales now increasingly incorporate other regional system components such as crops, urban features and, of most relevance to the present study, hydrology.

### 1.3 A dynamical hydrometeorological model: WRF-Hydro modelling system

95 The Weather Research and Forecasting Model Hydrological modeling system (WRF-Hydro) is a model coupling framework designed to link multi-scale process models of the atmosphere and terrestrial hydrology (Gochis et al., 2018). It runs both in fully-coupled (two-way) or uncoupled (one-way, from atmosphere to land) modes and is intended to serve as both a hydrometeorological prediction system and a research tool. The system has been applied in studies around the world (e.g. Senatore et al. 2015; Givati et al. 2016; Arnault et al., 2016; Xiang et al., 2017; Naabil et al., 2017; Verri et al., 2017; Lin et al., 2018; Rummler et al., 2019). It is currently in use operationally as a key component of the United States national water model where it expands the number streamflow forecast points from ~3600 points to ~2.7 million river reaches (<https://water.noaa.gov/about/nwm>). WRF-Hydro has also been applied in Africa (Arnault et al., 2016; Kerandi et al., 2018), in the Himalayas (Li et al., 2017), in Italy (Verri et al., 2017; Senatore et al., 2015) and in Eastern Alps (Rummler et al., 2019) with promising results and shows potential for use in runoff forecasting, water resource planning and climate changes impact assessments. However, despite application across a diverse array of catchments and research questions, the system has yet to be evaluated for a case in Norway.

There are still challenges to discharge prediction by WRF-Hydro and the performance varies across geographic regions and climate. For example, it simulated flood events in the Black Sea region fairly well if both model calibration and WRF data assimilation were performed jointly, while the streamflow obtained with raw WRF precipitation was in general very poor (Yucel et al., 2015). It also simulated a full annual cycle of the Crati River basin in southern Italy with Nash-Sutcliffe Efficiency (NSE) of 0.8 using observed precipitation while only achieved an NSE of 0.27 using simulated precipitation (Senatore et al., 2015). Naabil et al. (2017) applied WRF-Hydro in a test case over west Africa for water resources management, and found that further improvements via proper model calibration and consideration of the effects of model biases in dam level were recommended, although model captured the attributes of the streamflow. Furthermore, Verri et al. (2017) demonstrated that the performance of WRF-Hydro was severely affected by various components including simulated precipitation, initial conditions and also the calibration / validation of discharge hydrography. In Texas, WRF-Hydro has shown promise as a forecast tool, but suffers from poor prediction skill in areas with human altered flows, in which both the surface runoff and the base flow are underpredicted (Lin et al., 2018). Additional studies also noted the sensitivity of WRF-Hydro to the initial conditions (spinup time) (Roman-Cascon et al., 2016; Bonekamp et al., 2018; Verri et al., 2017). In order to obtain a stable WRF-Hydro simulation, a spinup period is required, which depends on the quality of the model input and



soil data. Therefore, the impact of the spinup time needs to be assessed on per-case basis as it likely depends on local conditions.

#### 1.4 Objectives of the paper

Due to the traditional separation of hydrological and atmospheric modelling communities, significant gaps exist in our  
125 knowledge of the full-chain responses to hydrometeorological extremes, from circulation/transport of moisture to  
precipitation to discharge. WRF-Hydro is designed to link across these components and their characteristic scales to provide  
a modelling framework that can address these gaps (Gochis et al., 2018).

In this study, we employ WRF-Hydro in western Norway to investigate meteorological and hydrological processes driving  
the October 2014 flooding. To our knowledge, this is the first study using a complete meteorological-hydrological modelling  
130 approach to characterize a precipitation induced extreme flooding event in Norway. The causal mechanisms and evolution of  
this particular flood event are examined. In addition, we explore the sensitivity of the discharge to different initial conditions  
such as soil and snow.

The work uses the output of Pontoppidan et al. (2017) as its starting point for the simulation of the meteorological processes  
and the hydrological impact. As such, an offline configuration for the WRF-Hydro model is chosen. This is because we  
135 primarily aim to understand the flood event in the context of its hydrological response to the weather forcing and land  
surface conditions. Feedbacks between the atmosphere and land, though important, generate second order effects that likely  
have only small impact within such a short duration event. Also, the offline mode of WRF-Hydro system is preferable for  
our study as it provides a clearer interpretation of the results, identification of uncertainties in the water budget and  
assessment of sensitivity to critical parameters in the atmospheric and hydrological components (Li et al., 2017).

140 The remainder of the paper is structured as follows: after the introduction, a description of the study area and data is  
presented, followed by methods, including a description of the WRF-Hydro setup and experiment design, model calibration  
and benchmark evaluation. Results concentrate on the model calibration and benchmark evaluation, precipitation evaluation,  
and the impacts of initialization (spinup time) and prescribed snow cover are examined. Finally, the main conclusions are  
presented.

## 145 2 Study area and data

### 2.1 Study area

Our four study catchments are located in western Norway, where the landscape is dominated by steep orography and  
complex terrain due to the fjords and elevation varies from sea level to more than 2400m (Figure 1). The complex terrain  
both enhances the precipitation and generates large local differences in the precipitation distribution (e.g. Reuder et al. 2007,



150 Pontoppidan et al 2017). Norway is positioned at the exit region of the North Atlantic storm track, which brings low-pressure  
systems and associated frontal precipitation towards the west coast on a regular basis during autumn and winter. Western  
Norway is the wettest part of the country (Hanssen-Bauer and Førland, 2000) and annual precipitation exceeds 3000 mm in  
several places; but there is also high spatial variability. For example, Kvamskogen-Jonshøgdi (60.389 N and 5.964 E)  
records 3151 mm while Vossevangen (60.625 N and 6.426 E), which is only 36.6 km away, only receives 1280 mm (MET  
155 Norway, 2015) (see in Figure 1).

## 2.2 Hydro-meteorological conditions

October 2014 was wetter than usual in western Norway. The situation was maintained by an atmospheric river and the  
passage of multiple frontal systems with moderate to heavy precipitation. Two days before the flooding event, on the 26<sup>th</sup> of  
October, a low-pressure system with associated fronts passed over western Norway and delivered considerable amounts of  
160 precipitation. A cold front passed the area at midnight on the 27<sup>th</sup>, advecting colder and drier air into the area for a short  
period. Simultaneously, a disturbance over Scotland developed and moved towards Norway, leaving western Norway in the  
warm sector of an intensifying low-pressure system. Once again large amounts of precipitation fell from midday on the 27<sup>th</sup>  
to early evening on the 28<sup>th</sup>. The associated cold front passed the Bergen area in the afternoon and the precipitation intensity  
decreased with its passage. Due to the already saturated soil and several days with more or less continuous rainfall, the flood  
165 peaked in the Voss area in early evening of the 28<sup>th</sup> (Pontoppidan et al., 2017).

According to the NVE report made by Langsholt et al. (2015), there was shallow snow cover in high-altitude areas east of  
the catchments. In Voss however, where our four catchments are located, there was no snow in the snow depth water  
equivalent maps released by NVE. These maps are made from model simulations based on snow observations from NVE.  
Discharge in each of the study catchments was over the 50-year return level. On the 29<sup>th</sup> of October, the daily discharge  
170 record held since 1892 was broken at the Bulken station, located at the outlet of Vangsvatnet (Langsholt et al., 2015).

## 2.3 Observational data

We use 43 precipitation gauges from the Norwegian Meteorological Institute (MET Norway) situated in and around the  
catchments, with either hourly or daily precipitation data. Typically rain gauges in Norway are deployed at low elevations  
and in valleys resulting in skewed precipitation distributions. To rectify this, 11 HOBO rain gauges, which provide hourly  
175 data, were deployed at higher elevations in a transect from the coast to inland (Pontoppidan et al., 2017). A table with station  
details can be found in Pontoppidan et al. (2017). Catchment averaged precipitation is calculated as a mean of the rain  
gauges positioned within the affected catchment. Four discharge stations from NVE are used for WRF-Hydro model  
discharge calibration and validation (see Table 1). It should be noted that the drainage basin of the Bulken catchment



includes the catchments of Kinne and Myrkdalsvatn. Figure 1 shows the locations of the four catchments and the  
180 measurement sites of rainfall and discharge gauges.

### 3 Methods

#### 3.1 WRF domain design

The Advanced Research WRF (WRF-ARW) model version 3.9.1 is set up with two nested domains with spatial resolution of  
9 km and 3 km (Figure 1). The lateral boundaries are forced with the 6-hourly ERA-interim reanalysis with a spatial  
185 resolution of 0.75 degrees (Dee et al. 2011). The sea surface temperatures (SST) are also updated every 6 hours. The model  
is run with 40 vertical levels in all domains.

The choice of the microphysical scheme is important for precipitation. Previous studies of mountain precipitation using  
WRF have shown that the Thompson microphysical scheme (Thompson et al. 2008) performs well (Collier et al. 2013;  
Maussion et al. 2014; Rasmussen et al. 2011, 2014, Li et al. 2017), especially in areas with mixed hydrometeors because it  
190 computes cloud water, rain water, snow, graupel and ice. The scheme was also successfully used in a previous study on this  
specific event (Pontoppidan et al. 2018). The grid spacing in the outer domain is in the so-called “gray zone” (5-10 km)  
where convection may or may not be explicitly resolved; therefore, we tested the impact of the convection parameterization  
on precipitation. The results showed negligible differences between simulations with the convection scheme on and off. Here  
we present the results from the simulations with the convection parameterization turned off. The Yonsei University scheme  
195 (Hong et al., 2006) is used for the planetary boundary layer, the RRTM scheme for long wave radiation (Mlawer et al., 1997)  
and the RRTMG scheme for shortwave radiation (Iacono et al., 2008). The Noah Land Surface model (‘Noah LSM’,  
Mitchell et al. 2001) is used for surface scheme, which has a bulk layer simple canopy and snow model. In the Noah LSM,  
the snow cover area fraction within a model grid is determined as a function of snow water equivalent (SWE) using a  
generalized snow depletion curve. When snow is on the ground, the model considers a bulk snow-soil-canopy layer and  
200 computes surface temperature at each time step. The snow surface temperature for the snowpack is estimated in two steps.  
Firstly, the energy balance between the snowpack, top soil layer and the overlying air is calculated to obtain an intermediate  
temperature. This temperature can rise above freezing even when the model grid is fully covered with snow. Secondly, the  
effective temperature is adjusted by accounting for the fractional snow cover on the ground (Livneh et al., 2010).

Additional configuration details include a model time-step of 18 seconds over the inner domain and the use of spectral  
205 nudging to keep the large-scale flow consistent with the driving ERA-Interim reanalysis. This approach proved to be useful  
when reproducing extreme precipitation events due to the better resolved synoptic scale features over North Atlantic  
(Heikkilä et al., 2011). Spectral nudging (Radu et al., 2008) is only applied in the outer domain leaving the model free to



create its own structures in the inner domain. In the present case, nudging is only applied above the boundary layer and only on wavelengths longer than 585 km.

### 210 3.2 WRF-Hydro modelling system

Version 3.0 of the WRF-Hydro modelling system is used in the study. A comprehensive description of the model system can be found in Gochis et al. (2015). In our study, the saturated subsurface overflow routing, surface overland flow routing, channel routing and base-flow modules are activated. The overland flow routing adopts a 2-D diffusive wave formulation (Julien et al., 1995) and the channel routing is calculated by a 1-D variable time-stepping diffusive wave formulation. In addition, a bucket model for base-flow is used where a groundwater reservoir with a conceptual depth and a related conceptual volume is associated. A few lakes in Bulken catchment are not considered in this study due to lack of data.

WRF-Hydro is set up to run offline using the WRF atmospheric simulations as input (see Introduction). The subgrid routing processes are executed at a 300m grid spacing and the surface physiographic files are prepared by ARCGIS 10.6 (Sampson et al. 2018). The physiographic file includes high-resolution terrain grids specifying the topography, channel grid, flow direction, stream order (for channel routing), ground-water basin mask and the position of stream gauging stations which are the outlets for water routing out across the landscape (Gochis et al., 2015). There are four stream orders in the network of the study catchments shown in Figure 2.

### 3.3 Model calibration

Two-step calibration of WRF-Hydro is performed in the study. First, we select the most sensitive parameters from a wide range of parameters. These include: the saturation soil conductivity (in SOILPARAM.TBL), optimum transpiration air temperature (in VEGPARAM.TBL) and infiltration parameter (in the surface runoff parameterization of GENPARAM.TBL), Manning roughness coefficients (in the channel routing of CHANPARAM.TBL), the groundwater bucket model exponent (in the ground water bucket model of GWBUCKPARAM.TBL), surface flow roughness scaling factor (OVROUGHRTFAC) and the surface retention depth (RETDEPRT) (Yucel et al., 2015; Li et al., 2017). Second, three parameters, which are particularly sensitive, are tuned using the auto-calibration Parameter Estimation Tool (PEST <http://www.pesthomepage.org>): two infiltration parameters, i.e. REFDK\_DATA (refdk) and REFKDT\_DATA (refkdt), which are important for surface runoff, and the Manning routing coefficients (mn01). The offline model is then forced by meteorological output data and calibrated based on the observed discharge in the Svartavatn catchment. The remaining three catchments (i.e. Bulken, Kinne and Myrkdalsvatn) are used for validation and evaluation of the parameters' transferability. The simulations are initialized on 1 September 2014 and run until 1 November 2014. In order to remove the impact of initialization we use the first 30 days as spinup in the model calibration. The best parameter set is then chosen based on the Nash-Sutcliffe efficiency (NSE)



coefficient (Nash and Sutcliffe, 1970). Two more indices, bias and root mean square error (RMSE) are also used for validation. A perfect model would have an NSE value of 1 and bias and RMSE values equal to 0.

### 3.4 Benchmark evaluation approach

240 A simple bucket-type Hydrologiska Byråns Vattenbalansavdelning (HBV) light model was used as a benchmark for model comparison and evaluation (Seibert and Vis, 2012; Seibert et al., 2018). The HBV light is an offshoot of the HBV model developed in the 1970s by the Swedish Meteorological and Hydrological Institute (SMHI). It consists of four main routines, i.e., snow-, soil-, routing- and response routine and simulates daily discharge using daily precipitation, temperature and potential evapotranspiration (Seibert and Vis, 2012). Its strength lies in the relatively low requirements for input data and the

245 limited number of parameters (Rusli et al., 2015). Here, the calibrated HBV streamflow is used as upper benchmark ( $R_{upper}$ ) and two alternatives are then used as lower benchmark ( $R_{lower}$ ), one generated from the mean streamflow from 1000 random parameter sets ( $R_{lower/random}$ ) and another from the regionalization parameter set from other nearby catchments ( $R_{lower/regional}$ ). The catchment averaged daily precipitation, temperature and potential evaporation from WRF are used as input in the HBV model simulation. To maintain consistency with the WRF-Hydro modeling, the HBV simulations are also initiated on 1

250 September 2014 and run until 1 November 2014 with the first 30 days used as spinup. The performance measure for the benchmark evaluation is the NSE.

### 3.5 Initialisation experiments

Previous studies found that spinup time influences the initial conditions such as the soil moisture content and therefore the latent heat flux, which in turn influences the precipitation (Kleczek et al., 2014; Bonekamp et al., 2018; Verri et al., 2017).

255 Jankov et al. (2007) suggested the spinup time should be at least 12 h to prevent instabilities in WRF, but the recommended length most likely depends on the input quality and soil fields (Kleczek et al., 2017). For example, Bonekamp et al., (2018) found that precipitation is extremely sensitive to the spinup time in summer, with the best performance coming with 24 hours of spinup, while does not show a clear trend with increasing spinup time over 24 hours. For our study, it is not known *a priori* how the model simulation will be effected by the spinup time. So we conduct experiments with different spinup times

260 ranging from 1 day to 26 days, and investigate the influence of spinup time on the amount of precipitation, soil moisture and outlet discharge of the extreme event in the study. An overview of the initialization experiments performed in the paper is given in Table 2. The evaluation period is 23 - 31 October 2014, and includes a minor peak flow on the 24<sup>th</sup> of October before the major peak flows on 26<sup>th</sup> and 28<sup>th</sup>.



### 3.6 Prescribed snow cover experiments

265 In the October 2014 flood event, temperatures in the mountains were above freezing and the ground was bare. In other  
words, there was no layer of snow to act as a sponge and potentially affect the discharge. In a future warmer climate,  
however, rain-on-snow events are likely to increase, especially in mountainous areas of Norway (Vormoor et al., 2016).  
However, the potential impact of snow conditions on extreme flows is not well known. Therefore, we construct a series of  
hypothetical experiments for a primary check on this impact. The results can be helpful for filling this knowledge gap and  
270 dictating the flood generation processes for Norway, although we know this hypothetical case most likely will increase in  
eastern and northern Norway instead of western Norway.

In the study, we perform two types of snow experiments: (1) different uniform snow depths are applied over the entire study  
area (i.e., 0.1m, 0.5m, 1m and 2m) and (2) 1m of snow is imposed above certain elevations (i.e. 400m, 600m and 800m  
above sea level (a.s.l.)). The experiments are all performed with the calibrated parameter set. More details can be found in  
275 Table 3. We are mainly interested in evaluating the precipitation-snowmelt timing and snowmelt augmentation of the peak  
flow, if any. Therefore, we apply the prescribed snow cover fields in the restart file on the 25<sup>th</sup> of October 2014, which is  
from the 26-day spinup experiment. The area-elevation distribution in the four selected catchments is shown in Table 4. The  
Kinne and Myrkdalsvatn catchments are dominated by higher elevations with 48% and 44% of the area above 1000m a.s.l.,  
respectively, compared to 36% and 9% from Bulken and Svartavatn (Table 4).

## 280 4 Results

### 4.1 WRF-Hydro discharge calibration

Since calibration is computationally demanding we calibrate WRF-Hydro based on the discharge of Svartavatn, which is the  
smallest catchment in the study region. The remaining three catchments are used for model validation. The calibration and  
validation results are shown in Table 5. The Nash-Sutcliffe-Efficiency coefficient (NSE) of daily discharge increases from  
285 0.31 to 0.86, while the Bias and RMSE decrease from 6.74 to 0.56 and from 1.2 to 0.55, respectively. It indicates that the  
calibration greatly improves the representation of discharge over Svartavatn. The NSE values are 0.77, 0.80 and 0.76 from  
Bulken, Kinne and Myrkdalsvatn, which are satisfactory although they are slightly lower than the NSE of 0.86 from  
Svartavatn. The infiltration parameters (refdk and refkdt) and Manning routing coefficients (mn01) are calibrated by PEST  
auto-calibration approach to be  $3.82E-6$ , 0.63 and 0.18, respectively. The correlation coefficient values of mn01 and refdk,  
290 mn01 and refkdt, refdk and refkdt are -0.23, -0.16 and 0.90, respectively. We can see that there is a high correlation between  
two infiltration parameters of refdk and refkdt. Figure 3 shows the daily observed discharge (black line) and simulated WRF-  
Hydro discharge from four study basins using various refkdt values for the extreme event during 23 - 31 October, 2014. It  
can be seen that WRF-Hydro is sensitive to the infiltration parameter refkdt and the uncertainty of peak flow is related to the



parameters' uncertainties. The peak discharge decreases from 717, 309, 83 and 102 m<sup>3</sup>/s with REFKDT of 0.2 to 698, 217,  
295 81 and 85 m<sup>3</sup>/s with REFKDT of 2.0 at Bulken, Kinne, Svartavatn and Myrkdalsvatn basin, respectively. An increase of  
refkdt in WRF-Hydro modelling leads to a decrease in peak flow, while a slower recession limb in the hydrograph.  
The daily observed discharge and simulated discharge based on the calibrated parameter set and the non-calibrated parameter  
set from the four study catchments are plotted in Figure 4. The hydrographs show that the calibrated runs capture the peak  
timing and magnitude well in all four catchments and that calibration markedly improves these features. The water balance  
300 of the four study catchments is shown in Table 6, which shows that the discharge at the four study catchments is driven by  
intense rainfall, and the impact of evapotranspiration and the changes in snow depth water equivalent and soil moisture are  
minor.

#### 4.2 Benchmark evaluation

Furthermore, the benchmark model efficiencies are also shown in Table 5. Daily precipitation, temperature and potential  
305 evapotranspiration from WRF are used as input to the HBV light model in order to calculate benchmarks. For the upper  
benchmark (i.e. using calibrated parameters), the calibrated HBV model efficiency ( $R_{\text{upper}}$ ) of Svartavatn basin is 0.80. For  
the lower benchmarks, the HBV model efficiency is 0.43 when calculated from random parameters ( $R_{\text{lower/random}}$ ) and is 0.67  
when calculated from regionalized parameter sets based on three nearby catchments ( $R_{\text{lower/regional}}$ ). Regarding the Bias and  
RMSE values, they are -0.42 and 9.03 from calibrated WRF-Hydro, 2.52 and 11.3 from the upper benchmark, and 7.56 /  
310 2.95 and 18.43 / 14.13 from two lower benchmarks ( $R_{\text{lower/random}}$  /  $R_{\text{lower/regional}}$ ). These results show that the calibrated WRF-  
Hydro model NSE of 0.86 is well above the upper benchmark (0.80). Besides, the calibrated WRF-Hydro has both less bias  
and smaller RMSE than the upper benchmark. Despite this encouraging result some care must be taken in the interpretation  
due to uncertainty in the input data for the HBV simulation caused by a lack of long-term averaged monthly meteorological  
forcing.

#### 315 4.3 Precipitation evaluation

The accumulated precipitation from 23 October at 06 UTC to 31 October at 06 UTC is shown in Figure 5. The CTRL  
simulation (see Table 3) is shown in colored contours and the observed values in colored squares (circles) for the HOBO rain  
gauge (meteorological) observational network. The observed precipitation amounts correspond well with the model  
simulation at the majority of the stations. The spatial variability is large in the complex terrain with several areas receiving  
320 close to 500mm precipitation and some areas less than 100mm during the week.

The temporal evolution of simulated precipitation at monitoring locations is shown in Figure 6. Observational stations are  
depicted in Figure 6a and the simulated precipitation interpolated from the four nearest grid points in the CTRL simulation is



shown in Figure 6b. Daily precipitation values are shown as diamonds, whereas hourly values are shown as continuous lines. The temporal evolution is generally well reproduced by the simulation, as well as the timing of the precipitating periods.

#### 325 4.4 Sensitivity to spinup time

Five different spinup times are investigated in order to analyze the sensitivity of precipitation and discharge to the initial conditions (see list in Table 3). The same calibrated parameter set is used for all the spinup experiments.

During this event the western coast of Norway was exposed to a considerable amount of precipitation within a 4-day period. Further, the soil was already saturated after a wet October. This can be seen in Figure 7 which shows (a) the catchment  
330 averaged total soil moisture of the four catchments in the CTRL experiment (26d-spinup), (b) the averaged total soil moisture on 24 October, (c) the difference of soil moisture between the 1d-spinup and CTRL, and (d) the difference of soil moisture between the 12d-spinup and CTRL. Figure 7 indicates a sensitivity of soil moisture to spinup time although the differences are fairly small (-10 to 10 mm). In general, the soil becomes slightly more wet with increased spinup time.

In addition, we evaluate the temporal evolution of the precipitation for the spinup experiments. Figure 8 shows the  
335 accumulated precipitation interpolated from the four nearest grid points to the following four rain gauge stations, Øvstedal, Myrkdalen, Mjølfjell and Vossevangen. These are the official meteorological observational stations located in the catchments of Svartavatn, Myrkdalen, Kinne and Bulken, respectively. The precipitation sensitivity to spinup time is low in all catchments. At Øvstedal and Mjølfjell the precipitation is reproduced well, whereas the remaining two stations are somewhat biased. The model seems to be unable to catch the finer scale phenomena completely with a 3 km grid resolution  
340 especially over a small complex catchment such as Myrkdalvatn. This could be partly due to the combination of highly complex terrain and interactions with the Sogne Fjord, just to the north, that are missing in the simulation. Table 7 provides additional evidence of this, showing the mean absolute error (MAE) in the total accumulated precipitation and discharge. The differences in MAE of precipitation between the spinup experiments are negligible; we believe this is because of the large-scale nudging in the outer domain. Besides, there is no decrease in precipitation MAE with the spinup time increase in  
345 any of the stations, except Øvstedal. The averaged MAE of precipitation at all 54 observational stations in the area is around 50 mm. Especially in Kinne, the discharge MAE increases with the extending of the spinup time. This suggests that the model, even at 3 km grid spacing, struggles to fully reproduce the local-scale orographic effects in the complex terrain around Voss and Myrkdalen. A previous study in the high mountains of Asia, suggested that a sub-kilometer grid is needed for accurately estimating truly local meteorological variability (Bonekamp et al., 2018).

350 The temporal evolution of streamflow over the four catchments is shown in Figure 9, which shows the daily hydrograph of discharge for the four catchments with different spinup experiments. We want to keep this flood event completely in our spinup experiment, so we evaluate the period of 23 - 31 October. From the results, we can see that the precipitation amount and timing do not differ significantly between spinup times in any of the catchments. However, the discharge at the pre-flood



phase, which is 23–24 October, is more sensitive to the spinup time. For Svartavatn this sensitive phase even extends to the  
355 26<sup>th</sup>. This is because the initial condition of soil moisture affects the overland flow that dominates the discharge of this  
catchment. The pre-flood discharge moves closer to the observed discharge when we increase the spinup time from 1 day to  
26 days. In general, the peak flows are overestimated compared with the observations, except in the Svartavatn catchment.  
This is because we only calibrated the model in Svartavatn, and then used this calibrated parameter set in the simulation for  
the other three catchments, which perforce have poorer performance than the Svartavatn catchment.

#### 360 4.5 Sensitivity to prescribed snow cover

The dynamical modelling experiments of different snow conditions are based on the WRF-Hydro simulation with a 26-day  
spinup, which is labelled as the control (CTRL) in the snow experiments (Table 2). In these experiments, the snow depth and  
the water equivalent snow depth are changed in the 25th of October restart file and the simulations are restarted in offline  
mode. An overview of the snow experiments is presented in Table 3. To summarize: one set of experiments tests the  
365 sensitivity to varying snow depths while the other set of experiments tests the sensitivity to snow elevation. The temporal  
evolution of catchment averaged SWE is shown in Figure 10 and Figure 11. A decline throughout the simulation period is  
shown for all catchments. Unsurprisingly, the snowmelt is due to positive surface temperatures and precipitation. The  
experiments with the 0.5m, 1m and 2m snow depths have similar snowmelt behavior during 25 - 28 October. The snowmelt  
stops in all the snow experiments after 29 October, because of a drop in both rainfall and temperature (below 273K), which  
370 can be seen in Figure 10. More detailed information of the total snowmelt during 25 - 31 October under the different snow  
experiments is given in Table 8. From the table, we can see that, except for the 0.1m snow depth experiment where the added  
snow quickly melts away, the results from other three prescribed snow depth experiments (0.5, 1.0 and 2.0 m) are fairly  
similar, where the total water equivalent snow melt are 14 -16 cm in Svartavatn, 11-12 cm in Myrkdalsvatn, 11-12 cm in  
Kinne and 12-13 cm in Bulken. This is because the limit of melting snow is controlled by the temperature and precipitation  
375 and maximum of around 0.5 m snow will be melted away in this case. For the snow elevation experiment where 1 m of snow  
were added above the given ground elevation, the response is a result of the elevation of the catchments. In Kinne and  
Myrkdalsvatn there is little variation, around 8-11 cm of SWE is melting. Their average catchment height is so high that  
there is only a small difference in total SWE between the experiments, leading to similar response. For Svartvatn and Bulken  
the situation is different. The total SWE in the catchments vary between the experiments because of the lower catchment  
380 elevation, hence the resultant SWE melting varies between 2-16 cm for Svartvatn and 4-12 cm for Bulken.

Figure 12 shows the hydrograph of hourly discharge for the experiments where snow depth is modified uniformly over the  
entire area. From both Figures 9 and 12, we can see that the difference in melt between the shallowest and deepest snow  
depths is less than 2 cm, which suggests that snow depths beyond 0.5m did not contribute markedly to more discharge. The  
main contribution from the additional snow is to enhance the peak discharge in all the catchments. Also, the contribution



385 from melting snow is mostly confined to precipitating periods, which also coincides with higher temperatures. The fact that  
snow depths above 0.5m have little impact suggests that rain-on-snow can melt at most 0.5 m snow under this experiment  
design. The snowmelt discharge decreases after 29 October, which is preceded by a drop in both rainfall and surface  
temperature (below 273k). It is worthwhile to recall that the Noah LSM has a simple bulk snow-soil-canopy layer model.  
Previous studies have noted that there was a positive bias in snow surface energy in the Noah LSM, which resulted in an  
390 underestimation of snow water equivalent (SWE), and led to a reduced snow pack during winter and earlier snowmelt in  
spring (Jin and Miller, 2007; Jin and Wen, 2012; Niu et al., 2011). In our experiments this positive bias in snow surface  
energy in the Noah LSM together with energy from intense rainfall are probably used to melt snow directly, so that the warm  
snowpack doesn't retain any liquid water which can refreeze during the day before it runs away. In this case, we might see  
unrealistically high snowmelt and the snowpack would not act like a sponge and retain part of the rainfall. All in all, the  
395 snow experiments show that intense precipitation coinciding with higher temperature can result in up to 0.5 m of snow melt,  
which contributes to the peak flow. However, more work needs to be done in the future with more sophisticated multi-layer  
snow models to confirm the behaviour observed in these idealized experiments.

The effects of varying snow cover by altitude on daily discharge are shown in Figure 13. Here, we perform snow  
experiments where 1m of snow is imposed above certain elevations, i.e., 400, 600, and 800 m. Those prescribed snow covers  
400 are applied in the restart file on 25 October 2014, which is from the 26-day spinup experiment with calibrated parameter set.  
From Figure 13 we can see that (a) there are increases in snow-melt runoff with the elevation decreases from 800 m to 0 m;  
(b) the differences of snow-melt runoff among different experiments vary in different catchments, for example, the snow-  
melt runoff from 0 m and 800 m experiments show a large difference in catchment Svartavatn, while not much difference  
can be seen in catchment Kinne and Myrkdalsvatn. This is because varying the prescribed snow cover by elevation has a  
405 greater influence on the lower catchments, i.e., Svartavatn (with 61% of the area below 800 m), than the higher catchments  
such as Kinne and Myrkdalsvatn (with 69% and 71 % above 800 m, respectively). A more detailed quantitative estimate of  
the total water equivalent snow depth change during 25-31 October under different prescribed snow cover experiments is  
given in Table 8. It confirms the results in Figure 10 and Figure 11, with the first half-meter of the snowpack contributing the  
to the snowmelt. In addition, there is a greater SWE decrease in the lower elevation catchment Svartavatn (i.e., -0.16 m in  
410 the added 1 m snow experiment) than Kinne and Myrkdalsvatn catchments (i.e., -0.11 m in the added 1 m snow experiment),  
which are dominated by higher elevations.

## 5 Discussion and conclusions

In this study, we aimed to reproduce an extreme weather event in a region characterized by complex terrain. A dynamical  
hydrometeorological modeling system (WRF-Hydro) was employed for this purpose. A nested WRF atmospheric model, run



415 at convection permitting scales, was used to reproduce the meteorological event and provide precipitation forcing for a  
distributed hydrological model over a small domain encompassing four study catchments affected by extreme flooding. 3km  
grid spacing was used for the WRF atmosphere and land surface while a 300m grid spacing was used for the WRF-Hydro  
river routing. An auto-calibration tool was used for WRF-Hydro model calibration based on the daily discharge at  
Svartevatn, which is the smallest of the 4 catchments. The simulation of high-resolution precipitation and discharge were  
420 assessed based on observational data sets. Also, the sensitivity of the results to the spinup time and snow depth was  
investigated.

The results show that the precipitation from the 3km simulation generally agrees well with the rain gauges both in terms of  
temporal evolution and spatial variability, although it underestimates the precipitation in the highly complex terrain around  
Myrkdalen. This underestimation could be due to a combination of the locally complex topography and the proximity to the  
425 Sognefjord only 15 km away. This large, but narrow body of water, and its many offshoots, is not well-resolved by the  
modeling system.

The auto-calibration greatly improves the model performance with the NSE increasing from 0.41 to 0.86, bias and RMSE  
decreasing from 5.29 and 19.05 to -0.42 and 9.03, respectively. The modeling system captures peak flow volumes and timing  
well after model calibration. Besides, WRF-Hydro runoff performance is depends on some highly sensitive parameters (e.g.  
430 infiltration parameter and Manning routing coefficients).

Comparing with the benchmarks, the calibrated WRF-Hydro NSE value (0.86) is higher than the upper benchmark from the  
HBV light model (0.80). This might be due a lack of long-term input data (e.g., averaged monthly potential  
evapotranspiration). The implication is that WRF-Hydro may perform as well or even better than a simpler conceptual  
hydrological model, especially for ungauged basins or observation scarce regions.

435 The precipitation simulation is not overly sensitive to spinup time. We find that mean absolute errors of precipitation are  
very similar given different spinup times. This could be due, in part, to the decision to nudge the atmospheric flow to match  
that large-scale reanalysis. Discharge simulations are slightly more sensitive to the spinup time due to the impact of soil  
moisture, especially during the pre-peak phase. We find a spinup time of 26 days give the lowest MAE of precipitation and  
discharge compared to the other smaller periods.

440 SWE melt during 25-31 October is consistently around 10 ~16cm for the uniform snow depth experiments (0.5 - 2 m). The  
results also show that melting snow contributes most to discharge during the rainy periods and the peak flow periods. This  
indicates that snow cover intensified the extreme discharge instead of acting as sponge in this study, which suggests that  
future rain-on-snow events may potentially result in higher flood risk. However, more sophisticated snow models and  
targeted experiments should be conducted to confirm this speculation.

445 Our results increase confidence in the performance of WRF-Hydro for simulating extreme hydrometeorological events over  
complex terrain. Further, they demonstrate the importance of model calibration and reasonably accurate land surface initial



conditions for simulating discharge, especially for peak flow. The snow experiments suggest that rain-on-snow events under warmer conditions may contribute to an increase in flood magnitudes in Norway, due to projected increases in extreme precipitation (Lawrence, 2016). However, targeted experiments on the changing risks associated with future rain-on-snow events are needed to confirm this possibility.

### Acknowledgments

This study was joint funded by the Research Council of Norway (RCN) project EVOGLAC (grant 255049), HordaKlim (grant 245403) and R3 (grant 255397), by the Bjerknes Center for Climate Research (SKD) project WACYEX and CHEX. The computer resources were available through the RCN's program for supercomputing (NOTUR/NORSTORE); projects NN9280K, NN9478K and NS9001K. All WRF-Hydro simulation data in this paper are available from the authors upon request (luli@norceresearch.no).

*Author contributions.* LL contributed to most of the modelling, analysis, writing and revising of the paper. MT contributed to collecting HOBO data, analysis and assisted with writing and reviewing the paper. SS contributed to the reviewing the paper. AS contributed to the model calibration by PEST and reviewing the paper.

*Competing interests.* The authors declare that they have no conflict of interest.

### References

- Arnault, J., Wagner, S., Rummler, T., Fersch, B., Bliefernicht, J., Andresen, S., & Kunstmann, H. (2016). Role of Runoff–Infiltration Partitioning and Resolved Overland Flow on Land–Atmosphere Feedbacks: A Case Study with the WRF-Hydro Coupled Modeling System for West Africa. *Journal of Hydrometeorology*, 17(5), 1489–1516. <https://doi.org/10.1175/JHM-D-15-0089.1>
- Avolio, E., Cavalcanti, O., Furnari, L., Senatore, A., and Mendicino, G. (2019). Brief communication: Preliminary hydro-meteorological analysis of the flash flood of 20 August 2018 on Raganello Gorge, Southern Italy, *Nat. Hazards Earth Syst. Sci. Discuss.*, <https://doi.org/10.5194/nhess-2019-62>, in review.
- Berghuijs, W. R., Woods, R. A., Hutton, C. J., & Sivapalan, M. (2016). Dominant flood generating mechanisms across the United States. *Geophysical Research Letters*, 43(9), 4382–4390. <https://doi.org/10.1002/2016GL068070>
- Bonekamp, P.N.J., Collier, E. and Immerzeel, W.W., 2018. The Impact of Spatial Resolution, Land Use, and Spinup Time on Resolving Spatial Precipitation Patterns in the Himalayas. *Journal of Hydrometeorology*, 19(10), pp.1565-1581.



- 475 Collier, E., Mölg, T., Maussion, F., Scherer, D., Mayer, C., & Bush, A. B. G. (2013). High-resolution interactive modelling of the mountain glacier–atmosphere interface: an application over the Karakoram. *The Cryosphere Discussions*, 7(1), 103–144. Dannevig et al., 2016, Naturfareprosjektet Oktoberflaumen på Vestlandet i 2014, rapport 2016-36, in Norwegian. Corripio, J.G. and López-Moreno, J.I., 2017. Analysis and Predictability of the Hydrological Response of Mountain Catchments to Heavy Rain on Snow Events: A Case Study in the Spanish Pyrenees. *Hydrology*, 4, 20.
- 480 Dee, D. P., and Coauthors, 2011: The ERA-Interim reanalysis: Configuration and performance of the data assimilation system. *Quart. J. Roy. Meteor. Soc.*, 137, 553–597, <https://doi.org/10.1002/qj.828>.
- Dyrørdal, A. V., Isaksen, K., Hygen, H. O., & Meyer, N. K. (2012). Changes in meteorological variables that can trigger natural hazards in Norway. *Climate Research*, 55(2), 153–165. <https://doi.org/10.3354/cr01125>
- Ek, M. B., K. E. Mitchell, Y. Lin, E. Rogers, P. Grunmann, V. Koren, G. Gayno, and J. D. Tarpley, 2003: Implementation of Noah land surface model advances in the National Centers for Environmental Prediction operational mesoscale Eta model. *J. Geophys. Res.*, 108, 8851, doi:10.1029/2002JD003296.
- 485 El-Samra, R., Bou-Zeid, E., & El-Fadel, M. (2018). What model resolution is required in climatological downscaling over complex terrain?. *Atmospheric research*, 203, 68–82.
- Freudiger, D., Kohn, I., Stahl, K., & Weiler, M. (2014). Large-scale analysis of changing frequencies of rain-on-snow events with flood-generation potential. *Hydrology and Earth System Sciences*, 18(7), 2695–2709. <https://doi.org/10.5194/hess-18-2695-2014>
- Givati, A., Gochis, D., Rummler, T. and Kunstmann, H., 2016. Comparing one-way and two-way coupled hydrometeorological forecasting systems for flood forecasting in the Mediterranean region. *Hydrology*, 3(2), p.19.
- Gochis, D.J., W. Yu, D.N. Yates, 2015: The WRF-Hydro model technical description and user's guide, version 3.0. NCAR Technical Document. 120 pages. Available at: WRF-Hydro 3.0 User Guide.
- 495 Gochis, D.J., M. Barlage, A. Dugger, K. FitzGerald, L. Karsten, M. McAllister, J. McCreight, J. Mills, A. RafieeiNasab, L. Read, K. Sampson, D. Yates, W. Yu, (2018). The WRF-Hydro modeling system technical description, (Version 5.0). NCAR Technical Note. 107 pages. Available online at <https://ral.ucar.edu/sites/default/files/public/WRF-HydroV5TechnicalDesc>. Source Code DOI:10.5065/D6J38RBJ
- 500 Hanssen-Bauer, I. and Førland, E., 2000. Temperature and precipitation variations in Norway 1900–1994 and their links to atmospheric circulation. *International Journal of Climatology: A Journal of the Royal Meteorological Society*, 20(14), pp.1693–1708.
- Hanssen-Bauer, I., Førland, E. J., Haddeland, I., Hisdal, H., Lawrence, D., Mayer, S., Ådlandsvik, B. (2017). Climate in Norway 2100.
- 505 Heikkilä, U., Sandvik, A. & Sorteberg, A. *Clim Dyn* (2011) 37: 1551. <https://doi.org/10.1007/s00382-010-0928-6>.



- Iacono, M. J., J. S. Delamere, E. J. Mlawer, M. W. Shephard, S. A. Clough, and W. D. Collins, 2008: Radiative forcing by long-lived greenhouse gases: Calculations with the AER radiative transfer models. *J. Geophys. Res.*, 113, D13103. doi:10.1029/2008JD009944.
- Jin, J. and Miller, N.L., 2007. Analysis of the impact of snow on daily weather variability in mountainous regions using MM5. *Journal of Hydrometeorology*, 8(2), pp.245-258.
- 510 Jin, J. and Wen, L., 2012. Evaluation of snowmelt simulation in the Weather Research and Forecasting model. *Journal of Geophysical Research: Atmospheres*, 117(D10).
- Julien, P., B. Saghafian, and F. Ogden, 1995: Raster-based hydrological modeling of spatially-varied surface runoff. *Water Resour. Bull.*, 31 (3), 523-536.
- 515 Hong, Song-You, Yign Noh, Jimmy Dudhia, 2006: A new vertical diffusion package with an explicit treatment of entrainment processes. *Mon. Wea. Rev.*, 134, 2318–2341. doi:10.1175/MWR3199.1
- Kendon, E. J., Ban, N., Roberts, N. M., Fowler, H. J., Roberts, M. J., Chan, S. C., ... & Wilkinson, J. M. (2017). Do convection-permitting regional climate models improve projections of future precipitation change?. *Bulletin of the American Meteorological Society*, 98(1), 79-93.
- 520 Kerandi, N., Arnault, J., Laux, P., Wagner, S., Kitheka, J., & Kunstmann, H. (2018). Joint atmospheric-terrestrial water balances for East Africa: a WRF-Hydro case study for the upper Tana River basin. *Theoretical and Applied Climatology*, 131(3–4), 1337–1355. <https://doi.org/10.1007/s00704-017-2050-8>
- Langsholt, E., Roald, L. A., Holmqvist, E., Fleig, A., 2015, Flommen på Vestlandet oktober 2014, NVE rapport 2015-11, in Norwegian.
- 525 Lawrence, D., 2016. Klimaendring og framtidige flommer i Norge. NVE Rapport nr. 81-2016.
- Mlawer, Eli. J., Steven. J. Taubman, Patrick. D. Brown, M. J. Iacono, and S. A. Clough, 1997: Radiative transfer for inhomogeneous atmospheres: RRTM, a validated correlated-k model for the longwave. *J. Geophys. Res.*, 102, 16663–16682. doi:10.1029/97JD00237.
- Li, L., Gochis, D. J., Sobolowski, S., & Mesquita, M. D. S. (2017). Evaluating the present annual water budget of a Himalayan headwater river basin using a high-resolution atmosphere-hydrology model. *Journal of Geophysical Research*, 122(9), 4786–4807. <https://doi.org/10.1002/2016JD026279>
- 530 Lin, P., Rajib, M.A., Yang, Z.L., Somos-Valenzuela, M., Merwade, V., Maidment, D.R., Wang, Y. and Chen, L., 2018. Spatiotemporal Evaluation of Simulated Evapotranspiration and Streamflow over Texas Using the WRF-Hydro-RAPID Modeling Framework. *JAWRA Journal of the American Water Resources Association*, 54(1), pp.40-54. <https://doi.org/10.1111/1752-1688.12585>
- 535 Livneh, B., Xia, Y., Mitchell, K.E., Ek, M.B. and Lettenmaier, D.P., 2010. Noah LSM snow model diagnostics and enhancements. *Journal of Hydrometeorology*, 11(3), pp.721-738.



- Marks, D., Kimball, J., Tingey, D., & Link, T. (1998). The sensitivity of snowmelt processes to climate conditions and forest cover during rain-on-snow: a case study of the 1996 Pacific Northwest flood. *Hydrological Processes*, 12(10–11), 1569–1587. [https://doi.org/10.1002/\(SICI\)1099-1085\(199808/09\)12:10/11<1569::AID-HYP682>3.0.CO;2-L](https://doi.org/10.1002/(SICI)1099-1085(199808/09)12:10/11<1569::AID-HYP682>3.0.CO;2-L)
- 540 Marks, D., Link, T., Winstral, A., & Garen, D. (2001). Simulating snowmelt processes during rain-on-snow over a semi-arid mountain basin. *Annals of Glaciology*, 32, 195–202. <https://doi.org/10.3189/172756401781819751>
- Maussion, F., Scherer, D., Mölg, T., Collier, E., Curio, J., & Finkelnburg, R., 2014. Precipitation Seasonality and Variability over the Tibetan Plateau as Resolved by the High Asia Reanalysis. *Journal of Climate*, 27(5), 1910–1927.
- 545 Lehner, F., Ikeda, K., Clark, M.P., Prein, A.F., Liu, C., Barlage, M. and Rasmussen, R., 2018. Projected increases and shifts in rain-on-snow flood risk over western North America. *Nature Climate Change*, 8(9), p.808.
- Mitchell, K. E., and Coauthors, 2001: The Community Noah Land Surface Model (LSM)—user’s guide (v2.2). Available online at [http://www.emc.ncep.noaa.gov/mmb/gcp/noahslm/README\\_2.2.htm](http://www.emc.ncep.noaa.gov/mmb/gcp/noahslm/README_2.2.htm).
- Naabil, E., Lamptey, B.L., Arnault, J., Olufayo, A. and Kunstmann, H., 2017. Water resources management using the WRF-Hydro modelling system: Case-study of the Tono dam in West Africa. *Journal of Hydrology: Regional Studies*, 12, pp.196–209.
- Nash, J. E. & Sutcliffe, J. V. 1970. River flow forecasting through conceptual models – Part 1 – A discussion of principles. *Journal of Hydrology* 10 (3), 282–290.
- Niu, G.-Y., and Coauthors, 2011: The community Noah land surface model with multiparameterization options (Noah-MP): 1. Model description and evaluation with local-scale measurements. *J. Geophys. Res.*, 116, D12109, <https://doi.org/10.1029/2010JD015139>.
- Pall, P., Tallaksen, L.M. and Stordal, F., 2018. A climatology of rain-on-snow events for Norway. In review with *Journal of Climate*. Available via EarthArXiv: <https://osf.io/k72ej/>
- 560 Pontoppidan, M., Reuder, J., Mayer, S., & Kolstad, E. W. (2017). Downscaling an intense precipitation event in complex terrain: the importance of high grid resolution. *Tellus A: Dynamic Meteorology and Oceanography*, 69(1), 1271561. <https://doi.org/10.1080/16000870.2016.1271561>
- Poschlod, B., Hodnebrog, Ø., Wood, R. R., Alterskjær, K., Ludwig, R., Myhre, G., & Sillmann, J. (2018). Comparison and Evaluation of Statistical Rainfall Disaggregation and High-Resolution Dynamical Downscaling over Complex Terrain. *Journal of Hydrometeorology*, 19(12), 1973–1982.
- 565 Prein, A.F., Langhans, W., Fossier, G., Ferrone, A., Ban, N., Goergen, K., Keller, M., Tölle, M., Gutjahr, O., Feser, F. and Brisson, E., 2015. A review on regional convection-permitting climate modeling: Demonstrations, prospects, and challenges. *Reviews of Geophysics*, 53(2), pp.323–361.
- Prein, A. F., Gobiet, A., Truhetz, H., Keuler, K., Goergen, K., Teichmann, C., ... & Vautard, R. (2016). Precipitation in the EURO-CORDEX 0.11° and 0.44° simulations: high resolution, high benefits? *Climate dynamics*, 46(1–2), 383–412.



- 570 Prein, A. F., Rasmussen, R. M., Ikeda, K., Liu, C., Clark, M. P., & Holland, G. J. (2017). The future intensification of hourly precipitation extremes. *Nature Climate Change*, 7(1), 48.
- Radu R, De 'que ´ M, Somot S (2008) Spectral nudging in a spectral regional climate model. *Tellus* 60A:898–910.
- Rasmussen, R., Liu, C., Ikeda, K., Gochis, D., Yates, D., Chen, F., ... & Gutmann, E., 2011. High-resolution coupled climate runoff simulations of seasonal snowfall over Colorado: a process study of current and warmer climate. *Journal of Climate*, 24(12), 3015-3048. doi: <http://dx.doi.org/10.1175/2010JCLI3985.1>
- 575 Rasmussen, R.M., K. Ikeda, C. Liu, D.J. Gochis, M. Clark, A. Dai, E. Gutmann, J. Dudhia, F. Chen, M.J. Barlage, D. Yates, and G. Zhang, 2014: Climate change impacts on the water balance of the Colorado headwaters: High-resolution regional climate model simulations. *Journal of Hydrometeorology*, 15, 1091-1116, DOI: 10.1175/JHM-D-13-0118.1.
- Reuder, J., Fagerlid, G. O., Barstad, I., Sandvik, A., 2007, Stord Orographic Precipitation Experiment (STOPEX): an overview of phase I, *Advances in Geosciences*, 10, 17-23. <https://doi.org/10.5194/adgeo-10-17-2007>.
- 580 Román-Cascón, C., G. Steeneveld, C. Yagüe, M. Sastre, J. Arrillaga, and G. Maqueda, 2016: Forecasting radiation fog at climatologically contrasting sites: Evaluation of statistical methods and WRF. *Quart. J. Roy. Meteor. Soc.*, 142, 1048– 1063, <https://doi.org/10.1002/qj.2708>.
- Rummler, T. et al., 2019: Role of Lateral Terrestrial Water Flow on the Regional Water Cycle in a Complex Terrain Region: Investigation With a Fully Coupled Model System. *JOURNAL OF GEOPHYSICAL RESEARCH-ATMOSPHERES* Volume: 124 Issue: 2 Pages: 507-529.
- 585 Rusli, S.R., Yudianto, D. and Liu, J.T., 2015. Effects of temporal variability on HBV model calibration. *Water Science and Engineering*, 8(4), pp.291-300.
- Sampson, K. and Gochis, D., WRF Hydro GIS Pre-Processing Tools, Version 5.0, Documentation, 2018.
- 590 Seibert, J. and Vis, M.J., 2012. Teaching hydrological modeling with a user-friendly catchment-runoff-model software package. *Hydrology and Earth System Sciences*, 16(9), pp.3315-3325.
- Seibert, J., Vis, M.J., Lewis, E. and Meerveld, H.V., 2018. Upper and lower benchmarks in hydrological modelling. *Hydrological Processes*.
- Senatore, A., Mendicino, G., Gochis, D. J., Yu, W., Yates, D. N., & Kunstmann, H. (2015). Fully coupled atmosphere-hydrology simulations for the central Mediterranean: Impact of enhanced hydrological parameterization for short and long time scales. *Journal of Advances in Modeling Earth Systems*, 7(4), 1693–1715. <https://doi.org/10.1002/2015MS000510>.
- 595 Smiatek, G., Kunstmann, H., & Senatore, A. (2016). EURO-CORDEX regional climate model analysis for the Greater Alpine Region: Performance and expected future change. *Journal of Geophysical Research: Atmospheres*, 121(13), 7710-7728.



- 600 Sorteberg, A., Lawrence, D., Dyrddal, A. V., Mayer, S., & Engeland, K. (2018). Climatic changes in short duration extreme precipitation and rapid onset flooding - implications for design values. Retrieved from [https://cms.met.no/site/2/klimaservicesenteret/rapporter-og-publikasjoner/\\_attachment/13537?\\_ts=163df95ff7b](https://cms.met.no/site/2/klimaservicesenteret/rapporter-og-publikasjoner/_attachment/13537?_ts=163df95ff7b)
- Stahl, K., Hisdal, H., Hannaford, J., Tallaksen, L. M., Van Lanen, H. A. J., Sauquet, E., ... Jódar, J. (2010). Streamflow trends in Europe: Evidence from a dataset of near-natural catchments. *Hydrology and Earth System Sciences*, 14(12), 2367–2382. <https://doi.org/10.5194/hess-14-2367-2010>.
- 605 Surfleet, C.G. and Tullos, D., 2013. Variability in effect of climate change on rain-on-snow peak flow events in a temperate climate. *Journal of hydrology*, 479, pp.24-34.
- Verri, G., Pinaridi, N., Gochis, D., Tribbia, J., Navarra, A., Coppini, G., & Vukicevic, T. (2017). A meteo-hydrological modelling system for the reconstruction of river runoff: The case of the Ofanto river catchment. *Natural Hazards and Earth System Sciences*, 17(10), 1741–1761. <https://doi.org/10.5194/nhess-17-1741-2017>.
- 610 Vormoor, K., Lawrence, D., Heistermann, M., & Bronstert, A. (2015). Climate change impacts on the seasonality and generation processes of floods – projections and uncertainties for catchments with mixed snowmelt/rainfall regimes. *Hydrology and Earth System Sciences*, 19(2), 913–931. <https://doi.org/10.5194/hess-19-913-2015>.
- Vormoor, K., Lawrence, D., Schlichting, L., Wilson, D., & Wong, W. K. (2016). Evidence for changes in the magnitude and frequency of observed rainfall vs. snowmelt driven floods in Norway. *Journal of Hydrology*, 538, 33–48. <https://doi.org/10.1016/j.jhydrol.2016.03.066>.
- 615 Wilson, D., Hisdal, H., & Lawrence, D. (2010). Has streamflow changed in the Nordic countries? - Recent trends and comparisons to hydrological projections. *Journal of Hydrology*, 394(3–4), 334–346. <https://doi.org/10.1016/j.jhydrol.2010.09.010>.
- 620 Xiang, T., Vivoni, E.R., Gochis, D.J. and Mascaro, G., 2017. On the diurnal cycle of surface energy fluxes in the North American monsoon region using the WRF-Hydro modeling system. *Journal of Geophysical Research: Atmospheres*, 122(17), pp.9024-9049.
- Yucel, I., A. Onen, K. K. Yilmaz, and D. J. Gochis, 2015. Calibration and evaluation of a flood forecasting system: Utility of numerical weather prediction model, data assimilation and satellite-based rainfall, *J. Hydrol.*, 523, 49–66.
- 625



**Table 1: The list of observed discharge stations**

Station	Area (km <sup>2</sup> )	Latitude	Longitude
Bulken(Vangsvatnet)	1092.04	6.29	60.63
Kinne	511.8	6.50	60.63
Svartavatn	72.3	5.90	60.65
Myrkdalsvatn	158.87	6.50	60.80

**Table 2: Overview of performed initialization experiments. All experiments are based on the calibrated parameter-set.**

Name	Spinup time
1d-spinup	1 day
3d-spinup	3 days
5d-spinup	5 days
14d-spinup	14 days
26d-spinup*	26 days

\*: 26d-spinup is used as the control (CTRL) experiment in the snow experiments.

630

**Table 3: Overview of pre-existing snow cover experiments. All experiments are performed during 25 - 31 October, based on the 26 days spinup simulation with calibrated parameter-set.**

Name	Added snow depth (m)	Added water equivalent snow depth* (m)	Elevation limits for adding snow** (a.s.l. m)
2m snow	2	0.67	0
1m snow	1	0.33	0
0.5m snow	0.5	0.17	0
0.1m snow	0.1	0.03	0
800m Elev	1	0.33	800
600m Elev	1	0.33	600
400m Elev	1	0.33	400
0m Elev	1	0.33	0

\* the snow density is assumed to be 300 kg/m<sup>3</sup>

\*\* the elevation limits for adding snow is 0 m, which means the snow is added over the whole catchment area.



635

**Table 4: Area-elevation of the four catchments**

>Elevation	400 m	600 m	800 m	1000 m
Bulken (%)	85	73	57	36
Kinne (%)	92	85	69	48
Svartavatn (%)	89	67	39	9
Myrkdalsvatn (%)	94	83	71	44

640 **Table 5: WRF-Hydro uncalibrated, calibrated, validated results with model efficiency values for different benchmarks**

	Catchment	NSE	Bias(mm)	RMSE(mm)
<b>Default (non-calibration)</b>	Svartavatn	0.41	5.29	19.05
<b>Calibration</b>	Svartavatn	0.86	-0.42	9.03
<b>Upper benchmark</b>	Svartavatn	0.80	2.52	11.30
<b>Lower benchmark (random parameter values)</b>	Svartavatn	0.43	7.65	18.43
<b>Lower benchmark (regional parameter values)</b>	Svartavatn	0.67	2.95	14.13
	Bulken	0.77	0.99	6.64
<b>Validation</b>	Kinne	0.80	-1.52	5.80
	Myrkdalsvatn	0.76	-0.005	6.65

**Table 6: The water balance of four study catchments during 25 - 31 October 2014 (based on calibrated parameter sets, unit: mm)**

Catchments	Observed Discharge	Precipitation	Discharge	ET	Soil water	Water equivalent snow depth	Residuals
------------	--------------------	---------------	-----------	----	------------	-----------------------------	-----------



Svartavatn	315	293.6	305.7	1.5	3.2	0.3	-17.1
Bulken	243.2	230.3	236.7	2.1	-2.5	0.9	-7
Kinne	187.6	206.6	219.8	1.2	-11.7	1.2	-3.9
Myrkdalsvatn	215	211.1	208	1.9	-14.7	0.6	15.3

645

**Table 7: Mean absolute error [mm] of precipitation and discharge compared with observations under impact of spinup time (23-31 October). The accumulated precipitation was interpolated from the four nearest grid points to Øvstedal, Myrkdalen, Mjølfjell, Vossevangen and (ALL) the 54 observational stations available in the area.**

MAE [mm]	spinup	Øvstedal (Svartavatn)	Myrkdalen (Myrkdalsvatn)	Mjølfjell (Kinne)	Vossevangen (Bulken)	ALL
<b>Precipitation</b>	1d	20	115	31	72	51
	3d	19	114	36	71	50
	5d	5	113	34	69	52
	12d	5	114	31	73	51
	26d	5	125	32	69	51
<b>Discharge (m<sup>3</sup>/s)</b>	1d	108	35	9	53	29
	3d	80	32	13	48	20
	5d	56	19	29	35	11
	12d	59	17	26	31	13
	26d	37	19	23	35	8

650

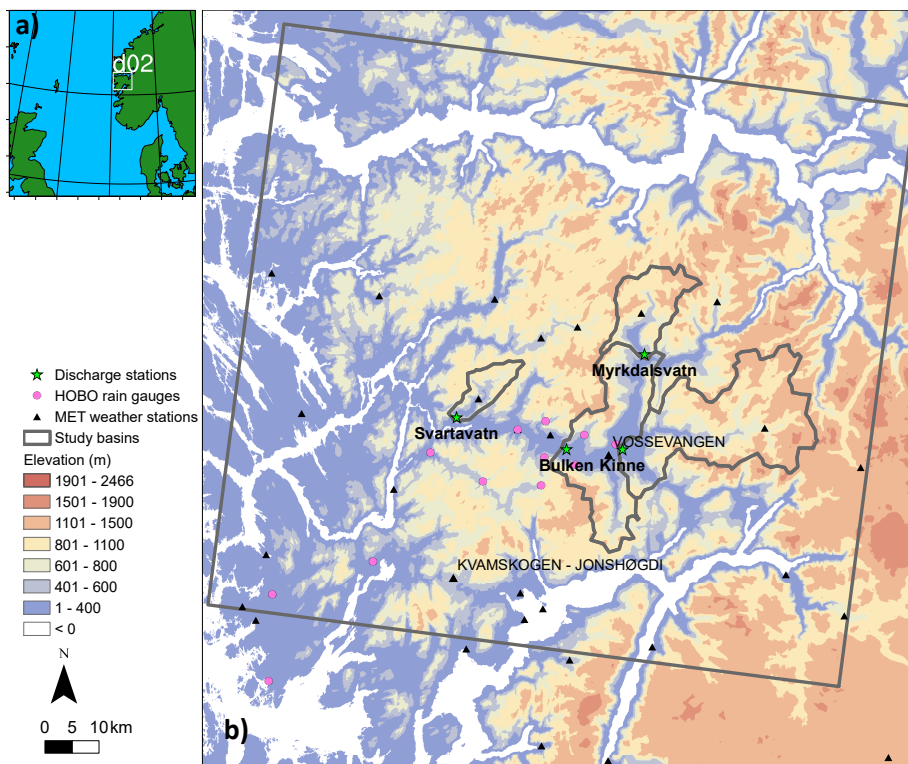
**Table 8: The total water equivalent snow depth change during 25-31 October under different pre-existing snow cover experiment in four study catchments.**



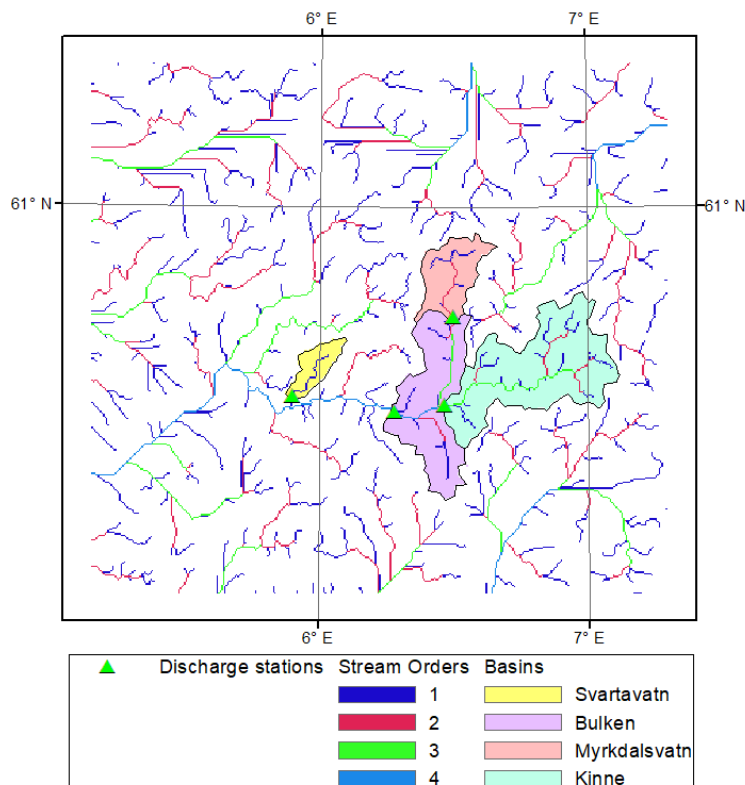
Experiments	Svartavatn	Myrkdalsvatn	Kinne	Bulken
CTRL	0.0004	0.0006	0.0014	0.0012
2m snow	-0.16	-0.12	-0.12	-0.13
1m snow*	-0.16	-0.11	-0.11	-0.12
0.5m snow	-0.14	-0.11	-0.11	-0.11
0.1m snow	-0.02	-0.02	-0.02	-0.02
800m Elev	-0.02	-0.08	-0.08	-0.04
600m Elev	-0.09	-0.09	-0.10	-0.09
400m Elev	-0.12	-0.11	-0.11	-0.11
0m Elev*	-0.16	-0.11	-0.11	-0.12

\*: 1m snow and 0m Elev are the same experiment.

655



660 **Figure 1:** The study catchments locate at western Norway. (a) Outer domain (resolution 9 km), borders of the inner domain (d02) are shown with a white frame; (b) zoom on the inner domain (resolution 3 km); topography and four study catchments boundaries are shown with details about ground-based observation stations, including discharge stations, HOB0 rain gauges and MET weather stations (from met.no), for model calibration and further performance evaluation.



665

Figure 2: Map of physiographic grid for routing processes with the four study catchments (i.e., Svartavatn, Bulken, Myrkdalsvatn and Kinne), the discharge stations and stream orders in the inner domain from hydrological modelling in WRF-Hydro model system. It is worth to note that the Bulken is at the downstream of Kinne and Myrkdalsvatn, which means the drainage basin of Bulken catchment comprises the catchment of Kinne (pink) and Myrkdalsvatn (light green) in the study.

670

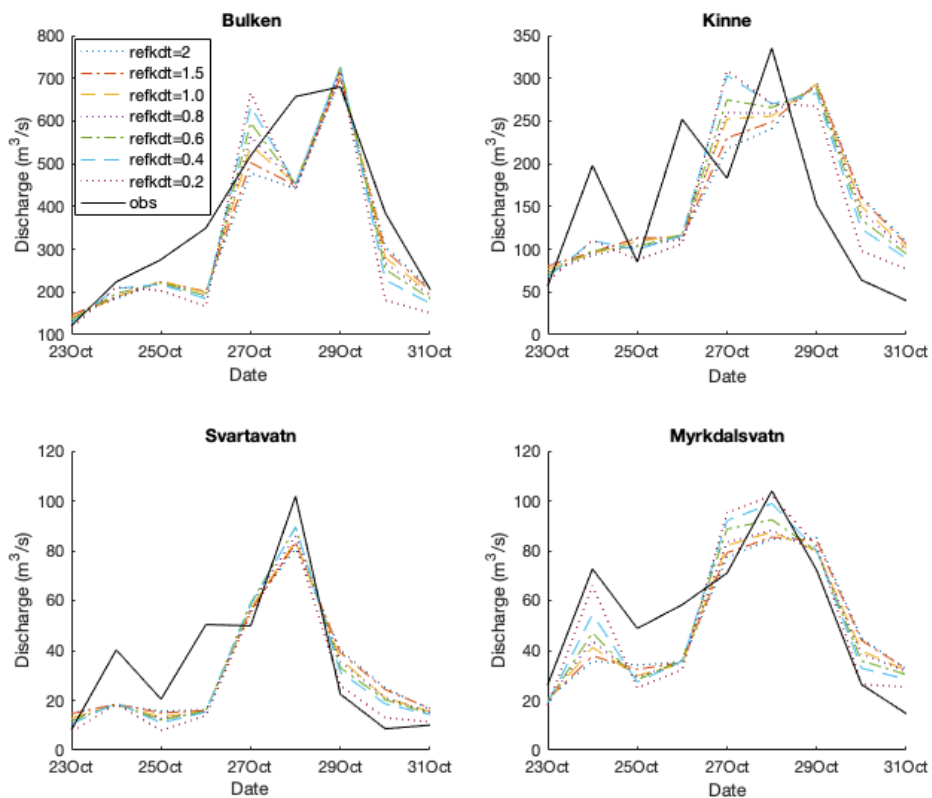
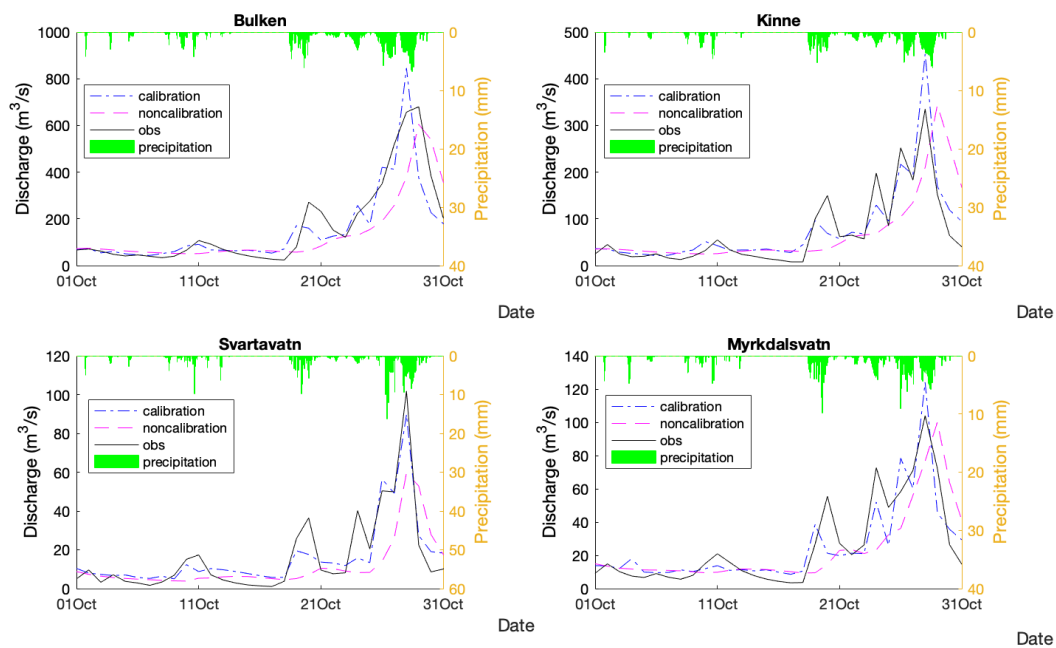
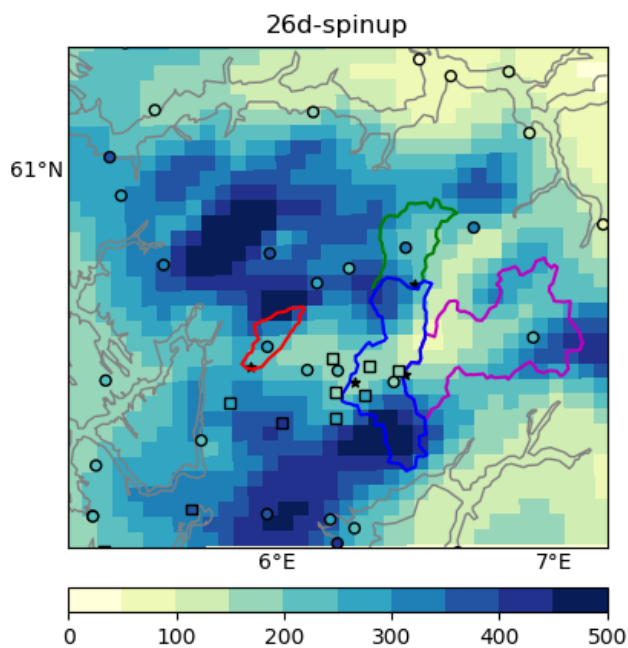


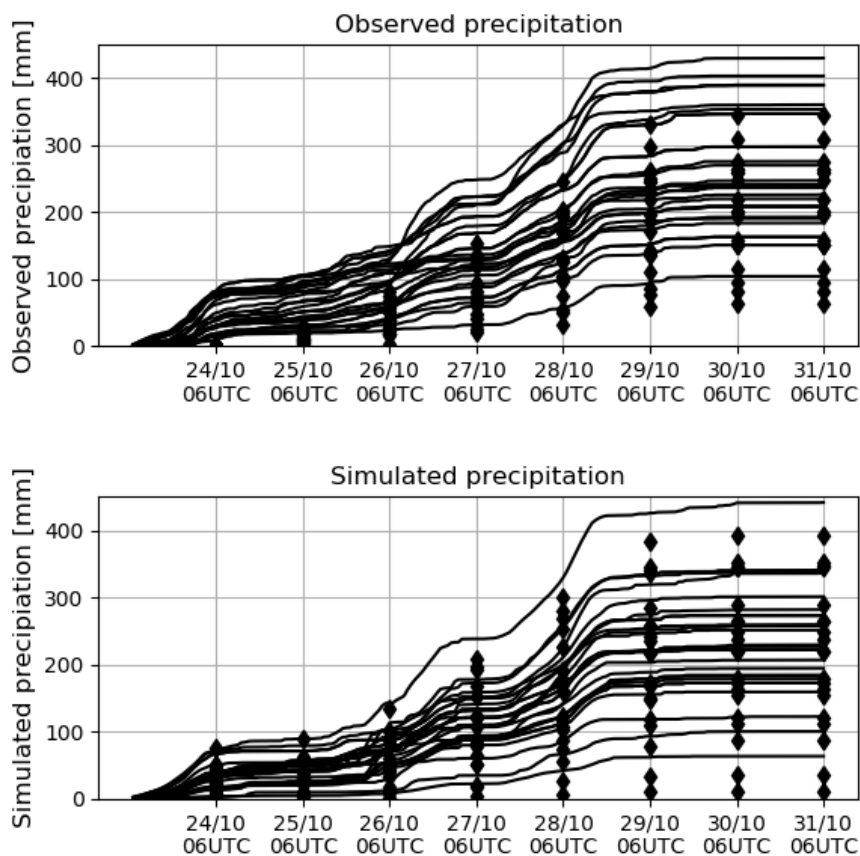
Figure 3: Hydrographs of daily observed discharge (obs) and simulated WRF-Hydro discharge from four study basins using various refkdt values for the extreme event during 23 - 31 October, 2014.



675 **Figure 4:** Hydrographs of daily observed discharge (obs) and simulated discharge with calibrated parameters (calibration) and non-calibrated parameters (noncalibration) with precipitation during 1 - 31 October, 2014.



680 Figure 5: Accumulated precipitation (mm) during 23 - 31 October from the 26 day spin up CTRL simulation. The catchments are  
contoured in colours corresponding to Figure 8. Squares and circles are observational values from the hobo network and the  
meteorological network respectively.



685 Figure 6: Accumulated precipitation from 23 October at 6 UTC to 31 October at 6 UTC a) at observation stations in the area and b) interpolated from the four nearest grid points to the equivalent station position in the 26d spin up simulation. The lines represent stations with hourly precipitation measurements whereas the diamonds represent stations with daily precipitation values. The same notation is used in b), though the model output enables higher temporal resolution at the daily station positions.

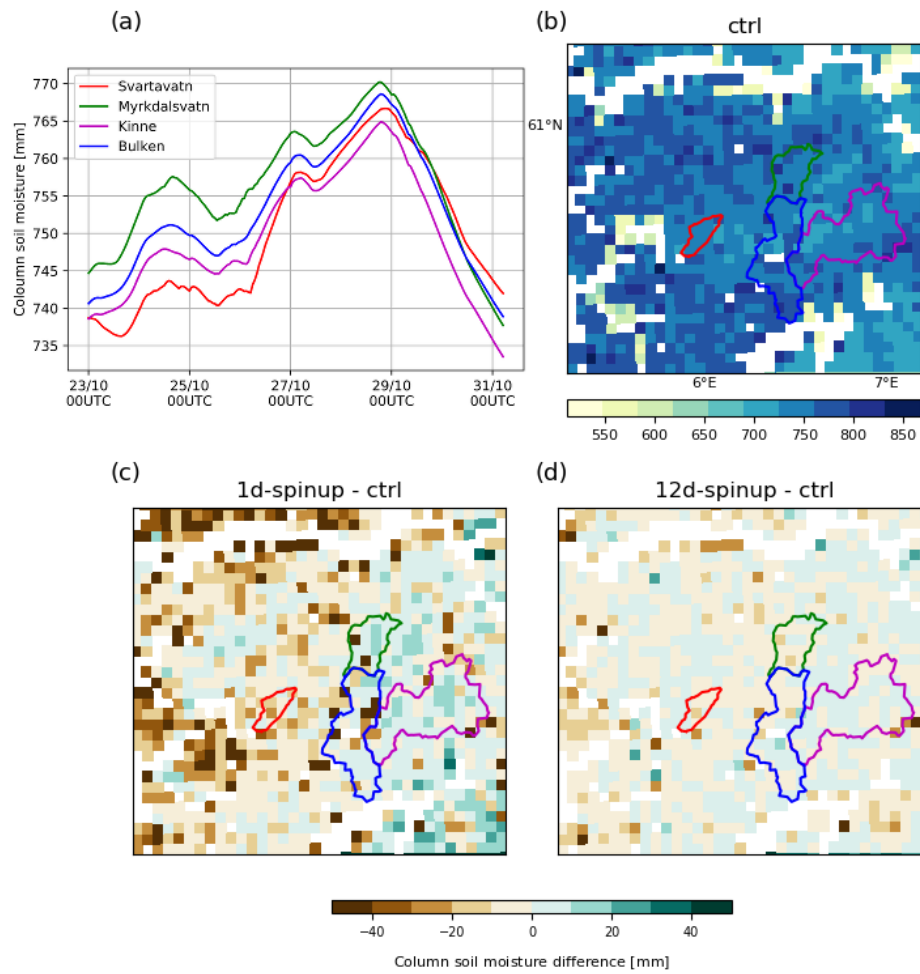
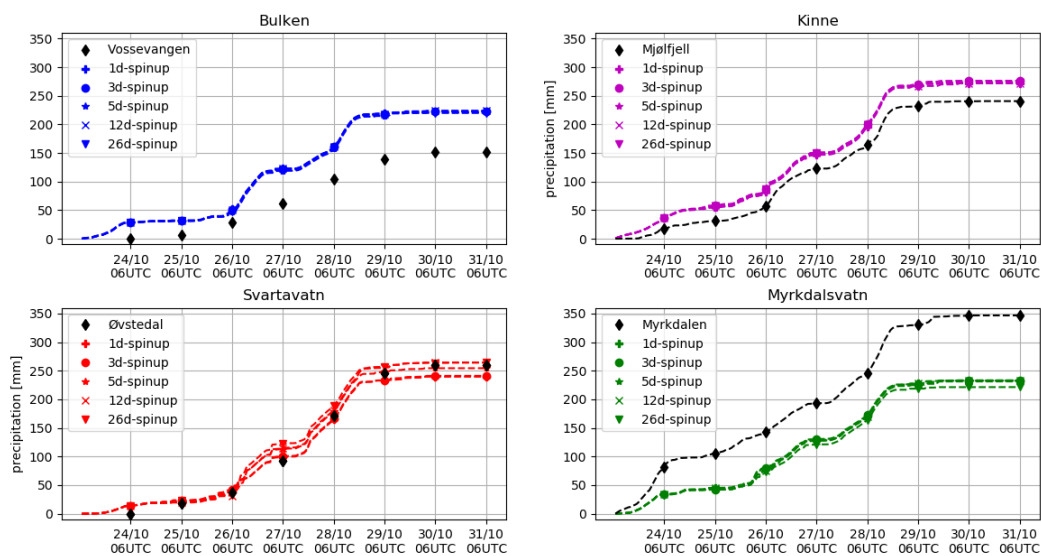
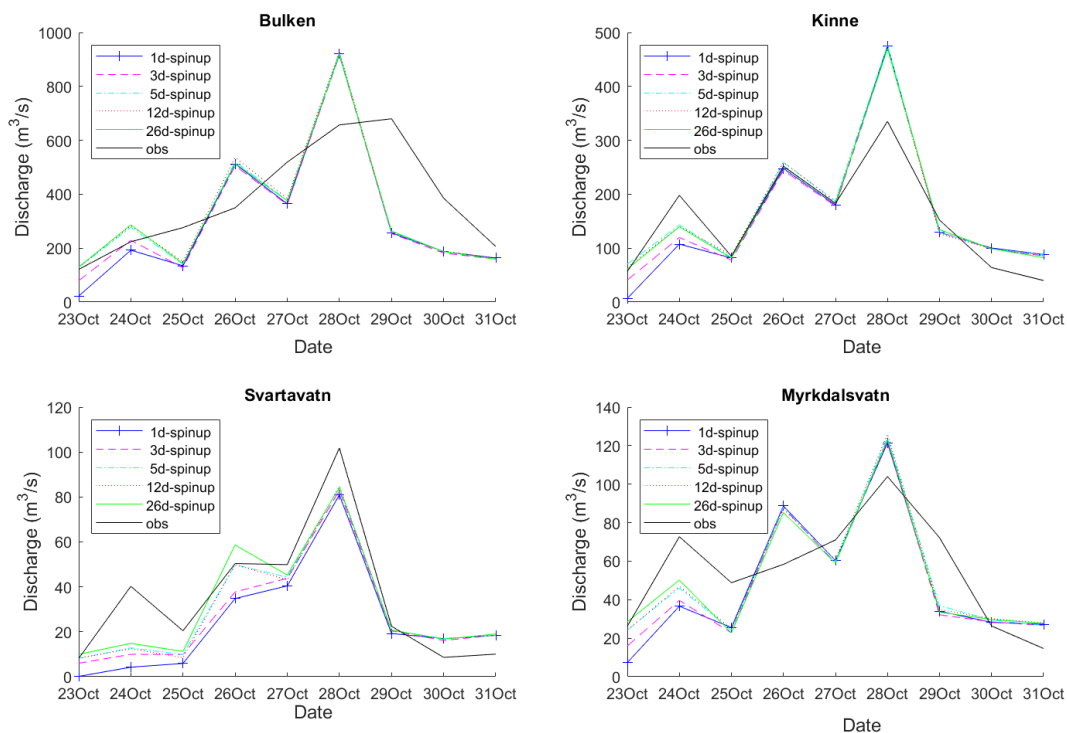


**Figure 7:** a) Temporal evolution of total column soil moisture averaged in the catchments (ctrl simulation); b) Averaged total column soil moisture on 24 October; c) soil moisture differences between the 1-day spinup and the control simulation; d) soil moisture difference between the 12-day spinup and the control simulation.



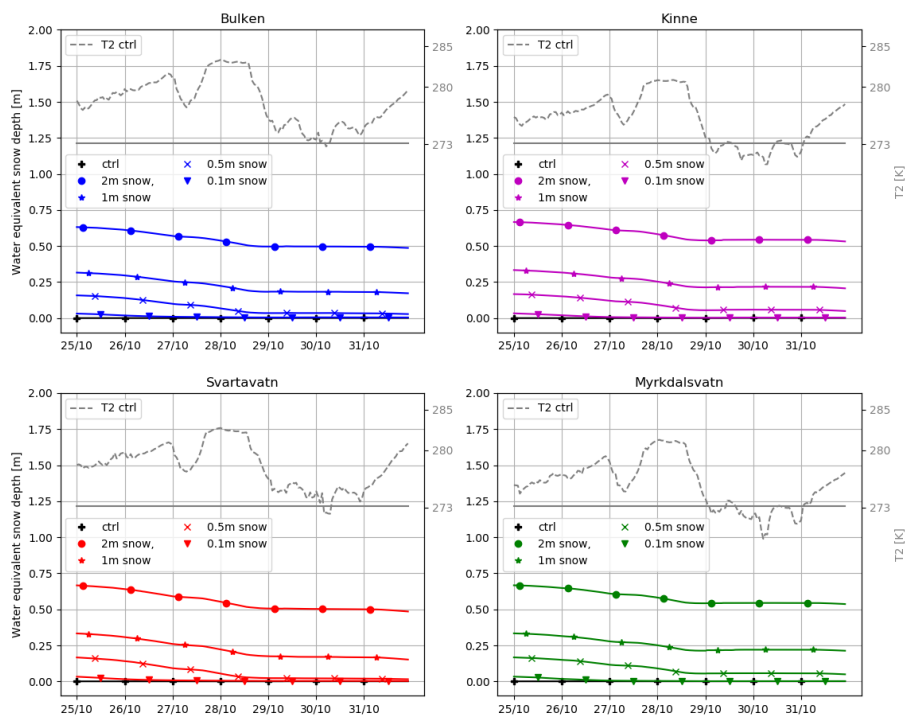
690

**Figure 8:** The accumulated precipitation from the simulations at the four nearest grid points to Vossevangen (Bulken), Mjølfjell (Kinne), Myrkdalen (Myrkdalsvatn) and Øvstedal (Svartavatn), observational stations from the simulations of different spinup times, including 1-day (1d-spinup), 3-day (3d-spinup), 5-day (5d-spinup), 12-day (12d-spinup) and 26-days (26d-spinup) compared with the observational station within the catchment.

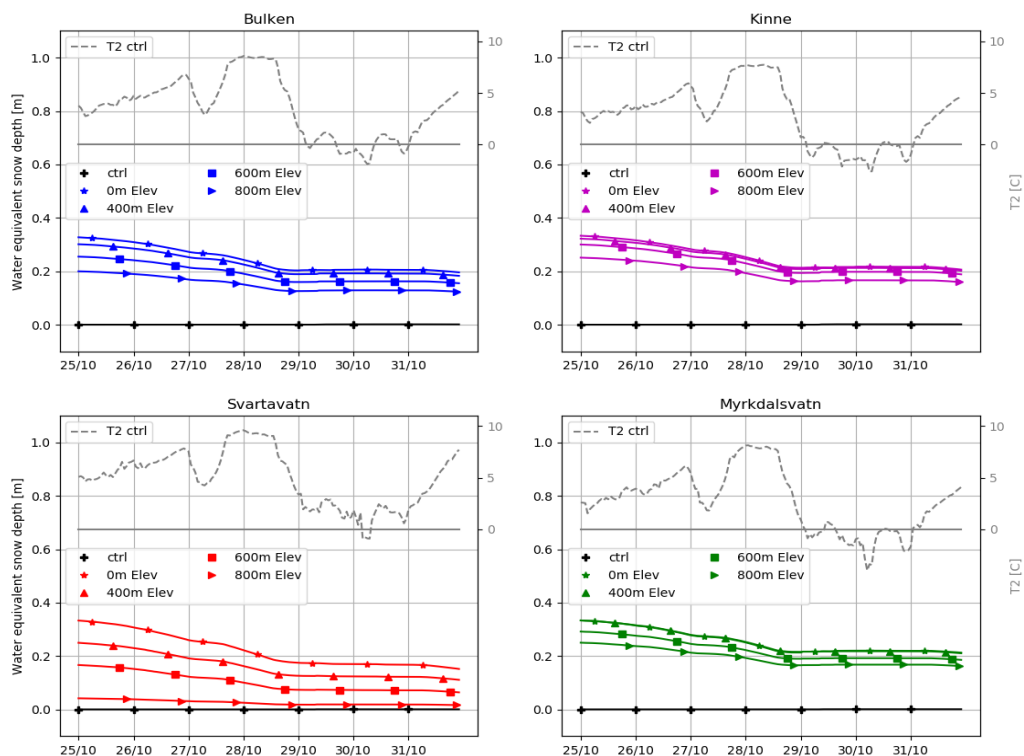


695

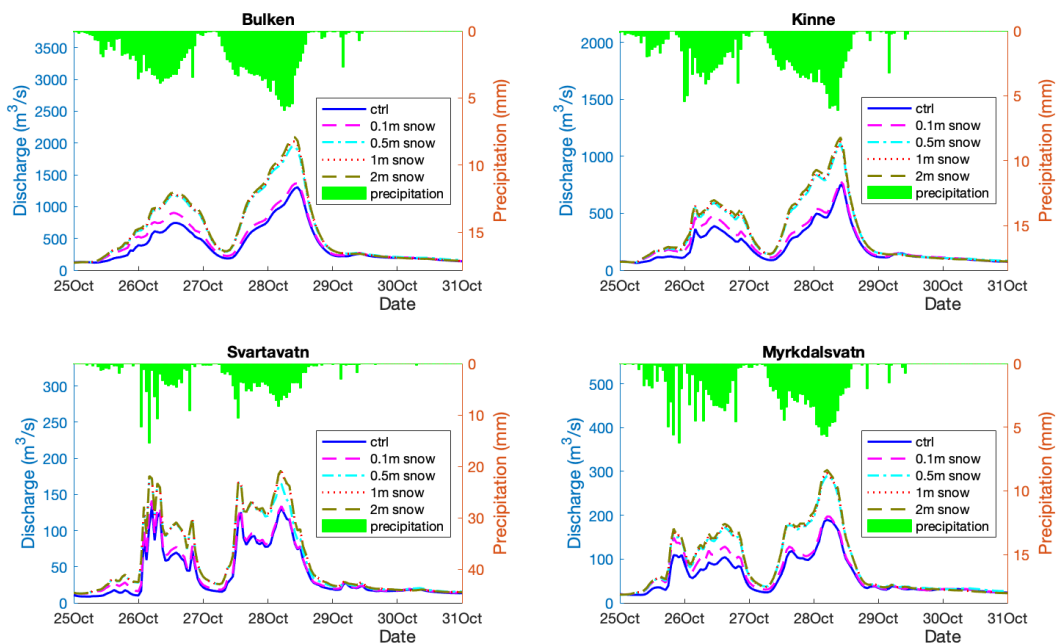
**Figure 9:** Daily observed streamflow (obs) and simulations discharges with different spinup time, including 1 day (1d-spinup), 3 days (3d-spinup), 5 days (5d-spinup), 12 days (12d-spinup) and 26 days (26d-spinup) for the flooding events during 23 - 31 October, 2014.



700 **Figure 10:** Catchment averaged hourly snow water equivalents from 3km WRF-Hydro simulation for the snow sensitivity experiments, including 2 m added snow depth (2m snow), 1 m added snow depth (1m snow), 0.5 m added snow depth (0.5m snow), 0.1 m added snow depth (0.1m snow), and the catchment averaged hourly snow water equivalent (ctrl) and surface temperature (T2) from the control simulation of the 26 day spinup.



705 **Figure 11:** Catchment averaged snow water equivalents from 3km WRF-Hydro simulation for the pre-existing snow cover sensitivity experiments, including 1 m added snow depth to the area where the elevation is above 0 m (0m Elev), 400 m (400m Elev), 600 m (600m Elev), and 800 m (800m Elev) based on the CTRL simulation (26 day spinup), and the catchment averaged hourly snow water equivalent (ctrl) and surface temperature (T2) from the control simulation of the 26 day spinup.



710 Figure 12: Hourly simulated discharge during 25 - 31 October from different experiments of added snow depths, i.e. 0.5 m, 1 m and 2 m snow and the control simulation from 26-day spinup without added snow depth (ctrl).

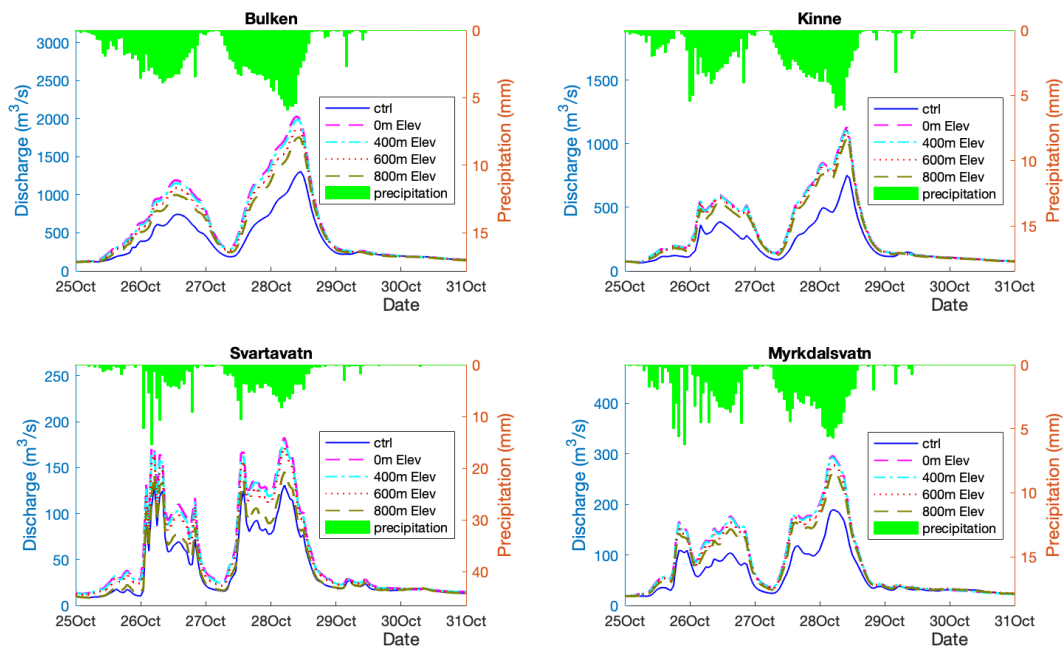


Figure 13: Hourly simulated discharge during 25 - 31 October from the control simulation (ctrl) and the different experiments of added 1m snow depths on the areas with elevation above 0, 400 m, 600 m and 800 m.